Liquid and Gas-Phase Distributions in a Jet With Phase Change

Flavio Dobran
New York University,
Applied Science Department,
New York, NY 10003

A two-phase flow high-velocity jet with phase change was studied numerically. The jet is assumed to be created by the two-phase critical flow discharge through a pipe of variable length and attached to a vessel containing the saturated liquid at different stagnation pressures. The jet flow is assumed to be axisymmetric and the modeling of the two-phase flow was accomplished by a nonequilibrium model that accounts for the relative velocity and temperature difference between the phases. The numerical solution of the governing set of balance and conservation equations revealed steep gradients of flow properties in both radial and axial directions. The liquid phase in the jet is shown to remain close to the jet axis, and its velocity increases until it reaches a maximum corresponding to the gas velocity, and thereafter decreases at the same rate as the gas velocity. The effect of decreasing the pipe length is shown to produce a larger disequilibrium in the jet and a double pressure peak in the total pressure distribution. A comparison of the predicted total pressure distribution in the jet with the experimental data of steam–water at different axial locations is demonstrated to be very reasonable.

1 Introduction

The discharge of a subcooled liquid at high pressure from a vessel through a pipe into an ambient atmosphere produces a rapid depressurization of the liquid and may produce two-phase critical flow at the discharge end of the pipe. Depending on the liquid stagnation conditions in the vessel and pipe geometric characteristics, the exiting two-phase mixture from the pipe may be in a considerable mechanical and thermal disequilibrium (Dobran, 1987). This disequilibrium is associated with the relative velocity and temperature difference between the phases, and may significantly affect the distribution of phases in the jet expansion region as the liquid and vapor are decelerated to the ambient conditions of the local atmosphere on the outside of the pipe. Due to the high momentum and pressure of the emerging two-phase mixture from the pipe, the expanding jet may create large forces on the surrounding objects, if they happen to be located in the vicinity of the jet discharge, and produce considerable loading on the pipe support structure and vessel to which the pipe is attached.

The purpose of this paper is to present a summary of results of the distribution of phases in the two-phase flow jet expansion region which were obtained by a nonequilibrium two-phase flow model of an axisymmetric jet with phase change. For the more extensive results of numerical simulations the reader is referred to Dobran (1985a, 1985b, 1985c, 1986). Section 2 of the paper deals with a brief description of the model, whereas in section 3 the results of a numerical study are presented and compared with data of the total pressure distribution at various positions along the jet.

2 Two-Phase Flow Jet Model and Solution Procedure

An axisymmetric two-phase flow configuration is illustrated in Fig. 1. The two-phase high-velocity jet exits from a pipe of diameter D and, upon encountering a low-pressure region surrounding the pipe, expands in the jet expansion region. The thermohydrodynamic conditions of the liquid and gas at the pipe exit are assumed to be known and the region surrounding the pipe is modeled as an ambient atmosphere at 0.1 MPa. The boundary conditions at the pipe exit must be determined by a critical two-phase flow model of sufficient generality in order to be able to predict reliably the detailed flow conditions at the exit. In this paper these boundary conditions were determined by a nonequilibrium critical flow model as described by Dobran (1987), which has been tested with the experimental data of steam–water for different stagnation pressures and liquid subcoolings in the vessel and for variable length pipes. The critical flow rates and tube exit pressures predicted by this model are shown to be within ±10 percent of the experimental values for wide range of fluid stagnation conditions and pipe geometric characteristics.

Governing Conservation and Balance Equations. For an axisymmetric flow configuration as depicted in Fig. 1, the governing conservation and balance equations of two-phase flow with phase change may be written in the following *conservation* form (Dobran, 1985a, 1985b):

$$\frac{\partial r\mathbf{f}}{\partial t}+\frac{\partial r\mathbf{F}}{\partial z}+\frac{\partial r\mathbf{G}}{\partial r}=r\mathbf{S} \tag{1}$$

where the vector $(r\mathbf{f})$ consists of the dependent variables, and the vectors $(r\mathbf{F})$, $(r\mathbf{G})$, and $(r\mathbf{S})$ depend on $(r\mathbf{f})$, i.e.

$$r\mathbf{f}=\begin{bmatrix} r\bar{\rho}_L \\ r\bar{\rho}_G \\ r\bar{\rho}_L u_L \\ r\bar{\rho}_L v_L \\ r\bar{\rho}_G u_G \\ r\bar{\rho}_G v_G \\ r\bar{\rho}_L[\epsilon_L+(u_L^2+v_L^2)/2] \\ r\bar{\rho}_G[\epsilon_G+(u_G^2+v_G^2)/2] \end{bmatrix} \tag{2}$$

Contributed by the Heat Transfer Division for publication in the JOURNAL OF HEAT TRANSFER. Manuscript received by the Heat Transfer Division February 9, 1987. Keywords: Jets, Multiphase Flows, Nonequilibrium Flows.

$$r\mathbf{F} = \begin{bmatrix} r\bar{\rho}_L u_L \\ r\bar{\rho}_G u_G \\ (r\bar{\rho}_L u_L)^2/(r\bar{\rho}_L) + r(1-\alpha)P \\ (r\bar{\rho}_L u_L)(r\bar{\rho}_L v_L)/(r\bar{\rho}_L) \\ (r\bar{\rho}_G u_G)^2/(r\bar{\rho}_G) + r\alpha P \\ (r\bar{\rho}_G u_G)(r\bar{\rho}_G v_G)/(r\bar{\rho}_G) \\ (r\bar{\rho}_L u_L)[\epsilon_L + (u_L^2+v_L^2)/2 + (1-\alpha)P/\bar{\rho}_L] \\ (r\bar{\rho}_G u_G)[\epsilon_G + (u_G^2+v_G^2)/2 + \alpha P/\bar{\rho}_G] \end{bmatrix} \quad (3)$$

$$r\mathbf{G} = \begin{bmatrix} r\bar{\rho}_L v_L \\ r\bar{\rho}_G v_G \\ (r\bar{\rho}_L u_L)(r\bar{\rho}_L v_L)/(r\bar{\rho}_L) \\ (r\bar{\rho}_L v_L)^2/(r\bar{\rho}_L) + r(1-\alpha)P \\ (r\bar{\rho}_G u_G)(r\bar{\rho}_G v_G)/(r\bar{\rho}_G) \\ (r\bar{\rho}_G v_G)^2/(r\bar{\rho}_G) + r\alpha P \\ (r\bar{\rho}_L v_L)[\epsilon_L + (u_L^2+v_L^2)/2 + (1-\alpha)P/\bar{\rho}_L] \\ (r\bar{\rho}_G v_G)[\epsilon_G + (u_G^2+v_G^2)/2 + \alpha P/\bar{\rho}_G] \end{bmatrix} \quad (4)$$

$$r\mathbf{S} = (r\mathbf{S}_1, r\mathbf{S}_2, r\mathbf{S}_3, r\mathbf{S}_4, r\mathbf{S}_5, r\mathbf{S}_6, r\mathbf{S}_7, r\mathbf{S}_8)^T \quad (5)$$

In the above equations the partial densities of liquid and gas are defined by

$$\bar{\rho}_L = (1-\alpha)\rho_L \quad (6)$$

$$\bar{\rho}_G = \alpha\rho_G \quad (7)$$

where α is the void fraction. The components of the vector ($r\mathbf{S}$) are reported by Dobran (1985a, 1985b) will not be reproduced here. The liquid and gas velocities consist of the components along the axis of the jet, u_L and u_G, and in the radial direction of the jet, v_L and v_G, as illustrated in Fig. 1.

Notice that the solution of $\mathbf{f} = \mathbf{f}(t, r, z)$ from equations (1) allows for the determination of the detailed two-phase flow conditions in the jet, since the liquid and gas densities are given by the equations of state, i.e.

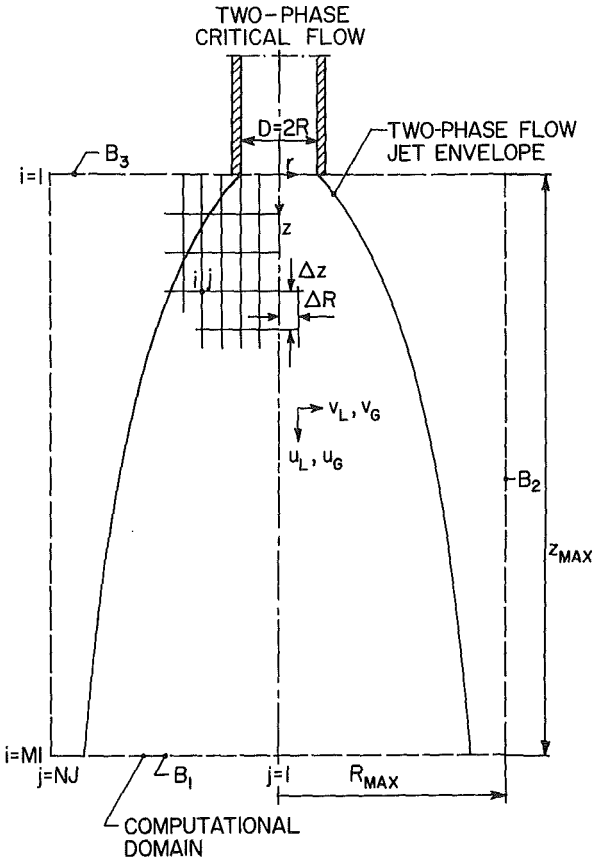

Fig. 1 Schematic illustration of the two-phase flow jet expansion region and computational mesh structure

$$\rho_L = \rho_L(P, \epsilon_L) \quad (8)$$

$$\rho_G = \rho_G(P, \epsilon_G) \quad (9)$$

For example, the liquid and gas velocities and internal energies may be found from the following relations:

$$u_L = \frac{(\bar{\rho}_L u_L)}{\bar{\rho}_L}, \quad v_L = \frac{(\bar{\rho}_L v_L)}{\bar{\rho}_L} \quad (10)$$

Nomenclature

A = interfacial area density, defined by equation (17)
Cp = specific heat at constant pressure
D = tube diameter
$\mathbf{f}$ = vector defined by equation (2)
$\mathbf{F}$ = vector defined by equation (3)
$\mathbf{G}$ = vector defined by equation (4)
G_o' = critical mass flux in the tube
i = computational node in the axial jet direction
j = computational node in the radial jet direction
k = thermal conductivity
L = pipe length
K = interfacial drag coefficient
N = droplet density
P = pressure
P_o' = stagnation pressure in the vessel to which the pipe is attached
Pr = Prandtl number
r = radial coordinate of the jet, Fig. 1
r_p = mean droplet radius, defined by equation (23)
$\tilde{R}$ = interfacial heat transfer rate, defined by equation (18)
R = pipe radius
Re = Reynolds number, defined by equation (22)
R_u = gas constant
$\mathbf{S}$ = vector, defined in Dobran (1985a, 1985b)
t = time
T = temperature
u = axial component of velocity
$\mathbf{U}$ = velocity vector
v = radial component of velocity
z = axial coordinate of the jet, Fig. 1
α = void fraction
Γ = evaporation or condensation rate, defined by equations (15) and (16)
ϵ = internal energy
λ = time relaxation parameter
μ = viscosity
ρ = density
$\bar{\rho}$ = partial density, defined by equations (6) and (7)

Subscripts

c = condensation
e = evaporation
G = denotes the gas or vapor phase
L = denotes the liquid phase
s = saturation condition

Table 1 Tube exit conditions computed by Dobran's (1987) critical two-phase flow model

Tube geometry		Stagnation conditions		Computed pipe exit conditions							
L/D	D, m	P_o', MPa	T_{sub}, °C	G_o', kg/m^2-s	P, MPa	α	u_L, m/s	u_G, m/s	$v_L = v_G$, m/s	ϵ_L, J/kg	ϵ_G, J/kg
300	0.0125	2.58	0	9294	1.094	0.914	120.5	120.5	0	8.35×10^5	2.58×10^6
100	0.0125	3.38	0	14,845	1.681	0.846	111.6	112.9	0	9.32×10^5	2.60×10^6

$$u_G=\frac{(\bar\rho_G u_G)}{\bar\rho_G},\quad v_G=\frac{(\bar\rho_G v_G)}{\bar\rho_G} \tag{11}$$

$$\epsilon_L=\frac{\bar\rho_L[\epsilon_L+(u_L^2+v_L^2)/2]}{\bar\rho_L}-\frac{1}{2\bar\rho_L^2}[(\bar\rho_L u_L)^2+(\bar\rho_L v_L)^2] \tag{12}$$

$$\epsilon_G=\frac{\bar\rho_G[\epsilon_G+(u_G^2+v_G^2)/2]}{\bar\rho_G}-\frac{1}{2\bar\rho_G^2}[(\bar\rho_G u_G)^2+(\bar\rho_G v_G)^2] \tag{13}$$

By eliminating the void fraction α in equations (6) and (7) and utilizing the equations of state (8) and (9) it is then possible to solve for the pressure from the following relation:

$$\bar\rho_L\rho_L(P,\epsilon_L)+\bar\rho_G\rho_G(P,\epsilon_G)=\rho_L(P,\epsilon_L)\rho_G(P,\epsilon_G) \tag{14}$$

and subsequently to determine the void fraction from either equation (6) or equation (7).

Equations (1) apply everywhere in the jet except along the jet axis where $r=0$. To obtain a valid set of equations along the axis it is necessary to divide equations (1) by r and take the limit $r\to0$ and recognize that $\mathbf{G}=\mathbf{0}$ at $r=0$.

Constitutive Equations. The closure of the balance equations (1) requires the specification of constitutive equations for the interfacial drag K, evaporation and condensation rates Γ_e and Γ_c, respectively, and the interfacial heat transfer rate $\tilde R$ contained in the source terms $\mathbf{S}$. The results of the numerical simulation presented below were obtained by assuming that the drag K is a constant and that the phase change process is controlled by the diffusion within the liquid and gas and not by the rate of energy exchange from the phase change. Under these conditions the evaporation and condensation rates are determined from the bulk liquid and vapor temperatures and may be written as (Solbrig et al., 1978):

$$\Gamma_e=\lambda_e A(1-\alpha)\rho_L\alpha(T_sR_u)^{1/2}(T_L-T_s)/T_s,\quad \text{for } T_L\ge T_s \tag{15}$$
$$=0,\ \text{otherwise}$$

$$\Gamma_c=\lambda_c A\alpha\rho_G(1-\alpha)(T_sR_u)^{1/2}(T_s-T_G)/T_s,\quad \text{for } T_G<T_s \tag{16}$$
$$=0,\ \text{otherwise}$$

where $\lambda_e=\lambda_c=0.1$ are the time relaxation parameters for evaporation and condensation with the unit of 1/s. For the equilibrium situation, the relaxation parameters are equal to one, whereas for very slow rates of phase change they would be equal to much less than one. The variable A in the above equations is proportional to the area of contact between the phases; for N equal size spherical droplets of radius r_p per unit volume, it is given by the following expressions:

$$A=\begin{cases}\alpha^{2/3}(4\pi N/3)^{1/3}, & \text{when } \alpha\le0.5\\ (1-\alpha)^{2/3}(4\pi N/3)^{1/3}, & \text{when } \alpha>0.5\end{cases} \tag{17}$$

A better model for the evaporation and condensation rates may be the one that assumes that these rates are controlled by the diffusion of energy from the bulk phases to the interface.

The interfacial heat transfer rate $\tilde R$ models the exchange of thermal energy between the liquid and gas. Its form is taken from the work of Solbrig et al. (1978), i.e.

$$\tilde R=\alpha\tilde R_G+(1-\alpha)\tilde R_L \tag{18}$$

where

$$\tilde R_G=(1+0.37\,\mathrm{Re}^{1/2}\mathrm{Pr}_G^{0.35})/r_p \tag{19}$$

$$\tilde R_L=8.067\,k_L/r_p \tag{20}$$

$$\mathrm{Pr}_G=\mu_G Cp_G/k_G \tag{21}$$

$$\mathrm{Re}=2r_p\rho_G|\mathbf{U}_G-\mathbf{U}_L|/\mu_G \tag{22}$$

$$r_p=\begin{cases}[3\alpha/4\pi N]^{1/3}, & \text{when } \alpha\le0.5\\ [3(1-\alpha)/4\pi N]^{1/3}, & \text{when } \alpha>0.5\end{cases} \tag{23}$$

and $N=10^{10}$ droplets/m^3 was assumed to be constant.

Initial and Boundary Conditions. The system of partial differential equations represented by equation (1) was solved in the computational domain as illustrated in Fig. 1 with the initial and boundary conditions specified in this domain. The computational region includes the two-phase flow jet envelope and extends sufficiently far into the radial and axial directions such that for $r>R_{max}$ and $z>z_{max}$ the initial flow field should not be significantly disturbed upon the introduction of the jet.

The initial flow configuration, or the local flow field configuration in the computational domain prior to the introduction of the jet, was assumed to consist of steam with the temperature and pressure equal to an air atmosphere, in which ambient conditions are given by $T_L=T_G=294$ K, $P=0.1$ MPa, $\alpha=0.999$, $\rho_L=935$ kg/m^3, $\rho_G=0.63$ kg/m^3, and $\mathbf{U}_L=\mathbf{U}_G=\mathbf{0}$.

The boundary conditions are specified at the tube exit and on boundaries B_1, B_2, and B_3 (see Fig. 1). At the tube exit the boundary conditions are determined by utilizing a suitable two-phase critical flow model. Table 1 summarizes these conditions for two different runs obtained by the critical flow model of Dobran (1987). The reason for selecting these runs is the availability of the experimental data of Celata et al. (1984) for the total pressure distribution in the jet, which can be used to determine the suitability of the jet model for the simulation of complex thermohydrodynamic processes within the jet. At the outflow boundary B_1 it is assumed that the flow properties in the jet do not vary significantly and that the jet properties can be determined by means of the second-order extrapolation of jet characteristics from the upstream points in the computational domain (Lapidus and Pinder, 1982). At the side boundary B_2 the boundary conditions are assumed to correspond to the initial conditions, except for the radial components of liquid and gas velocities, which are set equal to the corresponding values at one node away from B_2, i.e., at $j=NJ-1$ in Fig. 1. At the inflow boundary B_3 the liquid and gas densities, internal energies, radial components of velocities, and pressure are set equal to the initial conditions. The axial components of fluid velocities are set floating in order to allow for the mass transfer across B_3.

Numerical Procedure. The governing conservation and balance equations of two-phase flow (1) together with the initial and boundary conditions discussed above were solved numerically by the extended Lax's finite difference scheme (Lapidus and Pinder, 1982) until the steady-state jet profiles were obtained. This numerical procedure is first-order accurate in time and second-order accurate in space, and it has a dissipative mechanism built into it whose coefficient of ar-

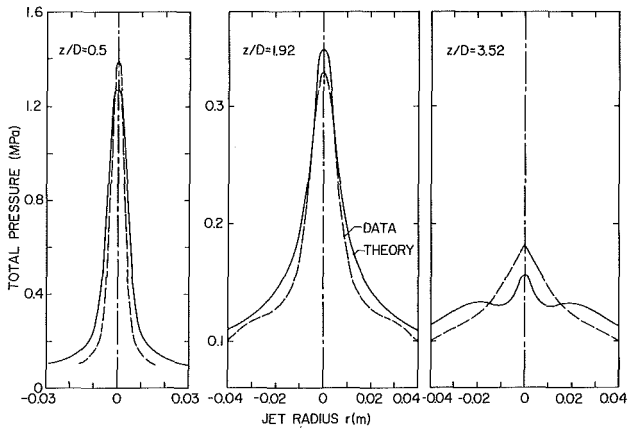

Fig. 2 Comparison of the predicted total pressure distribution in the jet with the experimental data of steam-water at various distances from the pipe end for L/D = 300, P_o' = 2.58 MPa, and ΔT_{sub} = 0°C

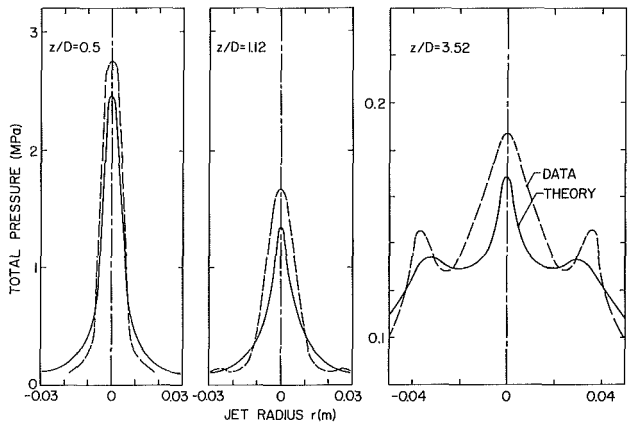

Fig. 3 Comparison of the predicted total pressure distribution in the jet with the experimental data of steam-water at various distances from the pipe end for L/D = 100, P_o' = 3.38 MPa, and ΔT_{sub} = 0°C

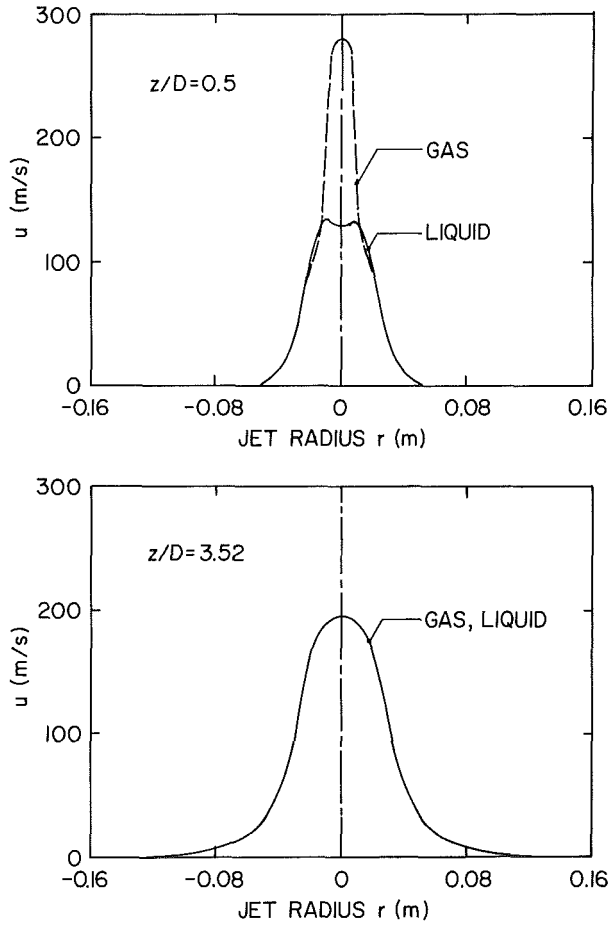

Fig. 4 Predicted distribution of the axial components of liquid and gas velocities in the jet for L/D = 300, P_o' = 2.58 MPa, and ΔT_{sub} = 0°C

tificial viscosity is proportional to $(\Delta z)^2/2\Delta t$. An accurate resolution of steep gradients in the jet, such as close to the pipe exit region, required, therefore, the use of the largest possible time step consistent with the Courant–Friedricks–Levy stability condition of the explicit finite difference methods. The discretized system of partial differential equations (1) was solved in the computational domain shown in Fig. 1, consisting of 40 radial and 60 axial nodes with nonuniform node separation as discussed in Dobran (1985b). The nonuniform node distribution was necessary in order to extend the computational domain in the radial and axial directions sufficiently far away from the steep gradients of flow properties close to the jet axis and tube exit. With this grid size specification and time step of 2×10^{-6} s, the steady-state conditions in the jet were established in a few ms. The effect of the mesh size on the accuracy of the computed variables was validated by a run with a uniform mesh size of 1.56 mm. When the computations were carried out with a variable mesh size as noted above it was established that such a small node separation was only necessary close to the jet centerline in order for the computed variables to remain within 3 percent accuracy in the entire computational domain.

3 Results and Discussion

Figures 2–6 illustrate the predicted steady-state pressure, velocity, and void fraction distributions in the jet at different axial positions corresponding to the two-phase flow pipe exit conditions in Table 1. Figures 2 and 3 show the predicted total or stagnation pressure distribution and a comparison with the experimental data of Celata et al. (1984). The stagnation pressure was computed according to the following equation:

$$P_{TOT} = P + 0.5[\alpha\rho_G u_G + (1-\alpha)\rho_L u_L]^2/[\alpha\rho_G + (1-\alpha)\rho_L] \quad (24)$$

As shown in Figs. 2 and 3, the predicted pressure distribution at different axial positions in the jet compares well with the steam-water data. The centerline pressure in the jet is underpredicted, whereas the jet spreading in the radial direction is overpredicted. Larger values of the interfacial drag K than the one used have the effect of producing a better comparison of the total pressure distribution in the jet with the experiment by increasing the centerline pressure and decreasing the radial jet dispersion. Nevertheless, the selected value of $K = 10^5$ kg/m^2-s was found to be very reasonable in predicting the radial and axial distributions of the total pressure and was used in producing all the results reported in the paper. The variation of other constants in the model (λ_c, λ_e, and N) by an order of magnitude from the selected values did not produce a practical change in the results reported in the paper.

At the axial position in the jet corresponding to $z/d = 3.52$, the predicted total pressure distribution exhibits a second peak for both runs in Table 1. For the two-phase flow situation in a long pipe (L/D = 300), the predicted second pressure peak is not as pronounced as for the flow through a shorter pipe (L/D = 100). Shorter tubes have the effect of producing larger mechanical and thermal disequilibrium at the tube exit (Dobran, 1987) as may be seen in Table 1, and this disequilibrium appears to be responsible for the occurrence of

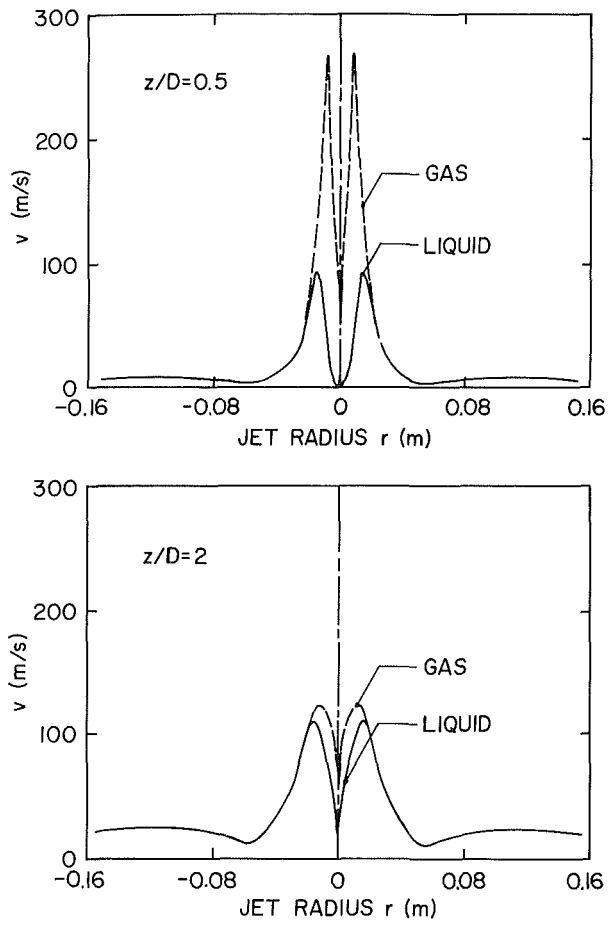

Fig. 5 Predicted distribution of the radial components of liquid and gas velocities in the jet for L/D = 300, P_o' = 2.58 MPa, and ΔT_{sub} = 0°C

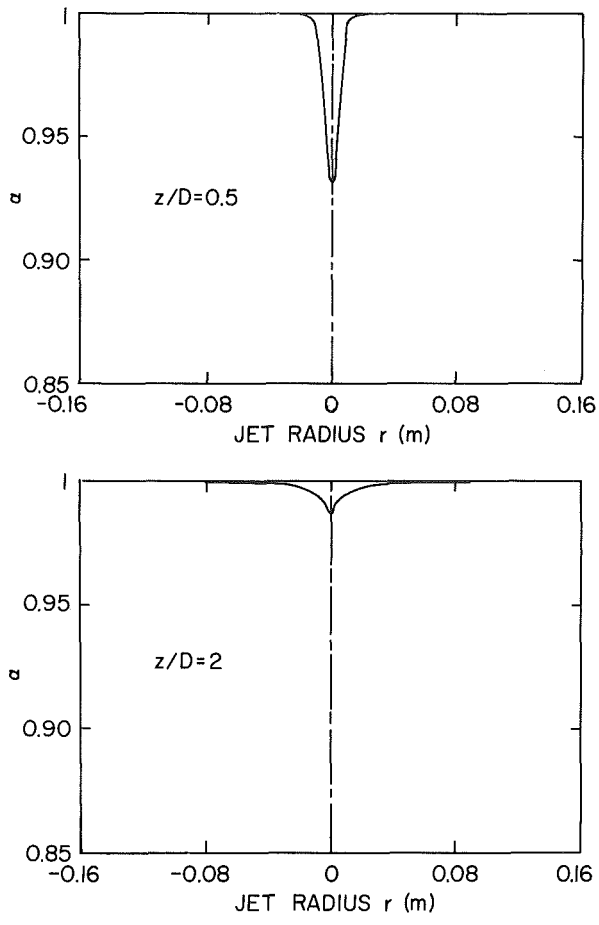

Fig. 6 Predicted void fraction distribution in the jet for L/D = 300, P_o' = 2.58 MPa, and ΔT_{sub} = 0°C

double pressure peaks of larger strengths. A pressure probe, such as pitot tube used to measure the total pressure distribution in the jet, may be responsible for the disturbance of the flow to such an extent that it may not yield an observation of a phenomenon such as a second pressure peak if this peak is of mild strength, as appears to be the case in Fig. 2 under the conditions of greater mechanical and thermal equilibrium. For the situation of $L/D = 100$ in Fig. 3, both the experiment and the theory show the occurrence of an off-axis pressure peak of sufficient strength.

An explanation of the foregoing observations on the total pressure distribution in the jet may be sought by examining the velocity and void fraction distributions in the jet. Figures 4 and 5 illustrate some typical distributions of the axial and radial components of velocity profiles at different positions in the jet. Close to the pipe end in the jet expansion region the gas velocity is seen to exceed substantially the liquid velocity, which may be attributed physically to the compressibility of the gas phase and to the finite value of the drag K. That is, as the gas and liquid exit from a pipe they encounter a zone of low pressure where only the gas phase can expand substantially. The liquid phase cannot, however, expand and its velocity can only increase as it is being dragged along by the gas. This explains why in Figs. 4 and 5 the gas-phase speeds in both axial and radial directions continue to decrease as the distance from the tube end is increased, and why at first the liquid velocity increases until it becomes equal to the gas velocity and thereafter it decreases at the rate corresponding to the gas velocity. The velocity vector plots of liquid and gas, shown in Dobran (1985b), serve to illustrate that the gas phase has a greater tendency (due to its lower inertia) than the liquid phase to move in the radial than in the axial direction. Indeed, the void fraction distributions in the jet illustrated in Fig. 6 confirm this observation, and are, furthermore, consistent with the qualitative x-ray measurements of Celata et al. (1985).

The profiles of the jet velocities illustrate that the selected computational domain discussed in the previous section is satisfactory, since the most significant changes of flow properties appear to occur well within this region. Another aspect of the numerical results is that the critical flows through shorter tubes (with the corresponding larger disequilibrium conditions at the tube exit) exhibit jet profiles of larger radial dispersion than for the longer tubes. This radial dispersion, as well as the remaining jet characteristics discussed above, are consistent with the experimental data of Celata et al. (1984) for steam-water jets discharging into an ambient air atmosphere.

4 Summary and Conclusions

A two-phase flow nonequilibrium model was used to study the distribution of liquid and gas in an axisymmetric jet with phase change, which is created by two-phase critical flow discharge through a pipe. The model assumes mechanical and thermal nonequilibrium between the phases, and the governing set of conservation and balance equations were solved by an explicit finite difference scheme until the steady-state jet characteristics were obtained. The numerical results predicted steep gradients of flow properties close to the pipe exit and along the jet axis, with the gas phase having the tendency to move more in the radial direction than the liquid phase. The total pressure distribution in the jet exhibits a double pressure peak: one at the jet centerline and another of lower amplitude off from the axis of the jet. The magnitude of the second

pressure peak may be associated with the degree of disequilibrium in the jet, since an increase in this disequilibrium has the effect of producing a larger radial dispersion of the gas phase and a correspondingly larger amplitude peak. A comparison of the predicted total pressure distribution in the jet with the steam-water data was shown to be very reasonable, both for the situations of radial and axial jet dispersion and the existence of double pressure peaks. The discrepancies between the numerical results and experimental data may be attributed to the uncertainties in the two-phase flow model and boundary conditions at the tube exit, as well as in simulating the ambient air atmosphere by a steam atmosphere. The numerical errors attributed to the artificial viscosity and variable grid size are judged to be minimal in view of the performed trial test with different grid sizes and time steps showing no practical changes in the results as presented in the paper.

References

Celata, G. P., Cumo, M., Farello, G. E., and Incalcaterra, P. C., 1984, "Physical Insight in the Evaluation of Jet Forces in LOCA," *Proc. 5th Int. Meeting on Thermal Reactor Safety*, Karlsruhe, Federal Republic of Germany, Sept. 10–13.

Celata, G. P., Cumo, M., and Farello, G. E., 1985, "X-Ray Analysis in Unbounded Two-Phase Critical Flows," *Specialists Meeting on Small Break LOCA Analyses in LWR's*, Giardini Editori e Stampatori, Pisa, Italy, Vol. 1, pp. 279–298.

Dobran, F., 1985a, "Analysis and Computation of Two-Phase Flow Jets With Phase Change," SIT Report No. ME-RT85010.

Dobran, F., 1985b, "Distribution of Liquid and Gas in a Jet With Phase Change," *Int. Symp. on Jets and Cavities*, J. H. Kim et al., eds., ASME, New York, pp. 49–56.

Dobran, F., 1985c, "Numerical Study of a Two-Phase Flow Jet," *Proc. 4th Int. Conf. on Numerical Methods in Thermal Problems*, R. W. Lewis and K. Morgan, eds., Pineridge Press, United Kingdom, Part 2, pp. 807–818.

Dobran, F., 1986, "The Effect of Liquid Subcooling and Tube Length on the Two-Phase Critical Flow in Tubes and Flow in the Jet," *Proc. 8th Int. Heat Transfer Conf.*, Hemisphere, New York, Vol. 5, pp. 2301–2306.

Dobran, F., 1987, "Nonequilibrium Modeling of Two-Phase Critical Flows in Tubes," ASME JOURNAL OF HEAT TRANSFER, Vol. 109, pp. 731–738.

Lapidus, L., and Pinder, G. F., 1982, *Numerical Solution of Partial Differential Equations in Science and Engineering*, Wiley, New York.

Solbrig, C. W., McFadden, J. H., Lyczkowski, R. W., and Hughes, E. D., 1978, "Heat Transfer and Friction Correlations Required to Describe Steam-Water Behavior in Nuclear Safety Studies," *AIChE Symp. Series*, Vol. 74, pp. 100–128.